Coherent sliding dynamics and spin motive force driven by crossed magnetic fields in a chiral helimagnet

Jun-ichiro Kishine
Division of Natural and Environmental Sciences, The Open University of Japan, Chiba 261-8586, Japan

I. G. Bostrem, A. S. Ovchinnikov, and Vl. E. Sinitsyn
Institute of Natural Sciences, Ural Federal University, Ekaterinburg 620083, Russia
(Received 1 November 2012; published 26 December 2012)

We demonstrate that the chiral soliton lattice formed from a chiral helimagnet exhibits a coherent sliding motion when a time-dependent magnetic field is applied parallel to the helical axis, in addition to a static field perpendicular to the helical axis. To describe the coherent sliding, we use the collective coordinate method and a numerical analysis. We also show that the time-dependent sliding velocity causes a time-varying Berry cap which creates a spin motive force. A salient feature of the chiral soliton lattice is the appearance of a strongly amplified spin motive force which is directly proportional to the macroscopic number of solitons (magnetic kinks).

DOI: 10.1103/PhysRevB.86.214426 PACS number(s): 75.47.−m, 75.30.−m, 85.75.−d

I. INTRODUCTION

Spin-based electronics (spintronics) is now an emerging field. An essential notion behind this emergence is the fact that the "spin magnetic current," which does not rely on an electric current, would greatly reduce the energy loss and switching time during information read-write processes. At the heart of spintronics is the requirement to drive the motion of magnetic textures in a controllable manner. There are two ways to drive the motion, i.e., incoherent and coherent methods.[1] The incoherent method is typically realized by injecting a spin-polarized current into a sample.[2] On the other hand, the coherent method is realized in a magnetically ordered state by twisting the phase angle of the magnetic order parameter which directly couples to a magnetic field. In the coherent method, the phase rigidity (stiffness) of the whole spin system makes it possible to transmit the spin rotation at one end of a sample to the other end via spin torque transfer. Although the coherent method has potential advantages, it has not been extensively studied in the context of present-day spintronics, because it is not so easy to prepare a rigid phase object which transports an experimentally measured quantity in a controllable manner. It is interesting to seek for the possibility of realizing the coherent method.

In this paper we propose that chiral helimagnets are promising candidates to realize the coherent method. The chiral helimagnetic (CHM) state is characterized by the vector spin chirality as an order parameter. The structure is stabilized by the antisymmetric Dzyaloshinskii-Moriya (DM) interaction and realized in crystals without rotoinversion symmetry. A guiding principle for materializing this effect is symmetry-adapted material synthesis, i.e., the interplay of crystallographic and magnetic chirality plays a key role there.

The CHM state is, however, nothing more than a non-collinear linear (harmonic) spin structure. To carry a physically measurable quantity, we need a nonlinear structure. Fortunately, under a magnetic field applied perpendicular to the helical axis, the CHM is transformed to a nonlinear magnetic structure called a chiral soliton lattice (CSL) (see Fig. 1), which is equivalent to a magnetic kink crystal.[3,4] In the CSL state, the ground state possesses a periodic array of commensurate and incommensurate domains partitioned by discommensurations. Recently, using Lorenz microscopy and small-angle electron diffraction, the CSL was experimentally verified in the hexagonal chiral magnet $Cr_{1/3}NbS_2$.[5] The present authors have discussed the physical possibilities of the CSL state from various viewpoints.[6–9]

As pointed out in Refs. 6 and 8, the CSL exhibits a coherent collective sliding motion in the nonequilibrium state. Once the sliding is triggered, the CSL maintains its persistent motion assisted by the dynamical generation of inertial mass. The mass generation can be understood by the Döring-Becker-Kittel mechanism of the moving domain wall.[10–12] In this mechanism, the longitudinal (out-of-plane) component of the slanted magnetic moment inside the domain wall emerges as a consequence of translational motion. An additional magnetic energy associated with the resultant demagnetization field is interpreted as the kinetic energy of the wall.

The incoherent current injection method to drive the sliding has already been proposed by the present authors.[9] In this paper, we demonstrate that crossed magnetic fields can cause the coherent motion of the whole CSL. Here, we mean "crossed fields" that in addition to a static field perpendicular to the helical axis, which stabilizes the CSL formation, a magnetic field parallel to the helical axis is imposed.

Once the coherent motion occurs, the natural question arises as to whether the motion has observable consequences for the spin motive force (SMF).[13] It is quite natural to expect that the time dependence of the longitudinal magnetic field manifests itself in the temporal regime of the SMF. The time dependence of the spin motive force can be classified into three types, i.e., (i) transient, (ii) continous ac, and (iii) continous dc. For example, domain wall motion[14] and electron transport through ferromagnetic nanoparticles[15] lead to type (i) SMF. Vortex core dynamics of a magnetic disk caused by an oscillating magnetic field directed in the disk plane induces a continous ac spin motive force of type (ii).[16] Resonant microwave excitation of a comb-shaped ferromagnetic thin film produces a continous dc spin motive force of type (iii).[17] We will demonstrate that the time-dependent longitudinal field, as shown in Fig. 1, possibly causes SMFs of types (i) and (ii) in the chiral helimagnet. As a remarkable feature, we note that our CSL is a macroscopically ordered

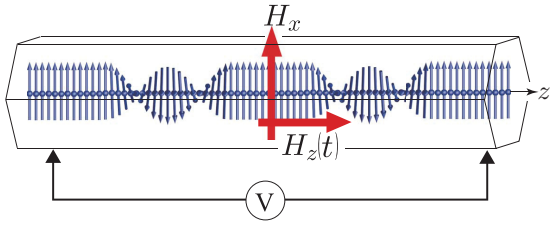

FIG. 1. (Color online) Schematic picture of the CSL. SMF generation needs a static transverse field H_x and a time-dependent longitudinal field H_x.

object, which contains macroscopic amounts of magnetic solitons. Due to this very large number of solitons, the SMF is expected to be strongly amplified as compared with the SMF caused by a single magnetic domain wall in a ferromagnet.

In Sec. II, we present the model and summarize the necessary background on the CSL dynamics. In Sec. III, we demonstrate that under the presence of the longitudinal field, the CSL becomes unstable and coherent motion occurs. In Sec. IV, we present a numerical analysis of the dynamics to support the analytical considerations presented in Sec. III. In Sec. V, we discuss the SMF associated with coherent motion. We give concluding remarks in Sec. VI.

II. STATIC DEFORMATION OF A CSL UNDER CROSSED MAGNETIC FIELDS

A. Basic equations of the chiral soliton lattice

1. Static structure

A monoaxial chiral helimagnet is described by an effective one-dimensional Hamiltonian,

$$H = -J\sum_i \boldsymbol{S}_i\cdot\boldsymbol{S}_{i+1} - \boldsymbol{D}\cdot\sum_i \boldsymbol{S}_i\times\boldsymbol{S}_{i+1} + \tilde{\boldsymbol{H}}\cdot\sum_i \boldsymbol{S}_i, \tag{1}$$

where $\boldsymbol{S}_i$ is the local spin moment at the site i, $J>0$ is the nearest-neighbor ferromagnetic exchange interaction, and $\boldsymbol{D}=D\hat{\boldsymbol{e}}_z$ is the monoaxial Dzyaloshinskii-Moriya interaction along a certain crystallographic chiral axis (taken as the z axis). We take the z axis as the monoaxis and apply the magnetic field $\tilde{\boldsymbol{H}}=g\mu_B\boldsymbol{H}=g\mu_B(H_x,0,H_z)$ in the xz plane, where g is the electron g factor and $\mu_B=|e|\hbar/2m$ is the Bohr magneton.

In the semiclassical approach, because of the slowly varying nature of the spin variables, it is legitimate to introduce the continuous field variable $\boldsymbol{S}(z)=\sum_i \boldsymbol{S}_i\delta(z-z_i)\equiv S\boldsymbol{n}(z)$. The unit vector field $\boldsymbol{n}(z)$ is represented as

$$\boldsymbol{n}(z)=[\sin\theta(z)\cos\varphi(z),\sin\theta(z)\sin\varphi(z),\cos\theta(z)], \tag{2}$$

by using the polar angles $\theta(z)$ and $\varphi(z)$. The continuum version of the Hamiltonian (1), $H=\int_0^L dz\mathcal{H}$, where L denotes the linear dimension of the system, includes the Hamiltonian density,

$$\mathcal{H}=\frac{JS^2}{2a_0}(\partial_z\boldsymbol{n})^2-\frac{S^2}{a_0^2}\boldsymbol{D}\cdot\boldsymbol{n}\times\partial_z\boldsymbol{n}+\frac{S}{a_0^3}\tilde{\boldsymbol{H}}\cdot\boldsymbol{n}. \tag{3}$$

Here a_0 is the atomic lattice constant along the chiral axis [$a_0\simeq 10$ Å in $Cr_{1/3}NbS_2$ (Ref. 5)].

For $\boldsymbol{H}=0$, the Hamiltonian (1) gives an xy-planar helimagnetic structure $\theta(z)=\pi/2$ and $\varphi(z)=Q_0z$ with the modulation wave number being given by $Q_0=a_0^{-1}\arctan(D/J)\simeq a_0^{-1}D/J$.

For a nonzero transverse field perpendicular to the chiral axis, the CSL structure becomes the ground state characterized by $\theta=\pi/2$ and

$$\varphi_0(z)=2\mathrm{am}\left(\frac{\pi Q_0}{4E}z\right),$$

where am is the Jacobi amplitude function with the elliptic modulus κ $(0\leqslant\kappa<1)$, and $E=E(\kappa)$ is the complete elliptic integral of the second kind. The elliptic modulus κ is determined from the condition

$$\kappa=\frac{4E}{\pi Q_0a_0}\sqrt{\frac{\tilde{H}_x}{JS}}. \tag{4}$$

This equation is also written as $\tilde{H}_x/\tilde{H}_c=(\kappa/E)^2$ by introducing the critical field corresponding to $\kappa=1$,

$$\tilde{H}_c=(\pi Q_0/4)^2JSa_0^2\sim D^2/J, \tag{5}$$

at which an incommensurate-to-commensurate phase transition occurs. The spatial period of the CSL is given by $L_{\mathrm{CSL}}=8KE/\pi Q_0$, which continuously increases from $L_{\mathrm{CHM}}=2\pi/Q_0$ to infinity when the magnetic field increases from zero to H_c. Here, $L_{\mathrm{CHM}}$is the spatial period of CHM under zero field. $K=K(\kappa)$ is the complete elliptic integral of the first kind.

2. Individual spin dynamics

Next, we write down the basic equations for the dynamics. Using the Hamiltonian density (3), we construct the Lagrangian density

$$\tilde{\mathcal{L}}=\frac{\hbar S}{a_0^3}(\cos\theta-1)\,\partial_t\varphi-\mathcal{H}. \tag{6}$$

To incorporate the damping effect, we use the Rayleigh dissipation described by

$$\tilde{\mathcal{W}}=\frac{\alpha\hbar S}{2a_0^3}(\partial_t\boldsymbol{n})^2 \tag{7}$$

with α being a small coefficient specifying the Gilbert damping. The Euler-Lagrange equations of motion are then given by

$$\frac{\hbar S}{a_0^3}\sin\theta\,\partial_t\theta=\frac{\delta\mathcal{H}}{\delta\varphi}+\frac{\delta\tilde{\mathcal{W}}}{\delta\dot{\varphi}}, \tag{8a}$$

$$\frac{\hbar S}{a_0^3}\sin\theta\,\partial_t\varphi=-\frac{\delta\mathcal{H}}{\delta\theta}-\frac{\delta\tilde{\mathcal{W}}}{\delta\dot{\theta}}, \tag{8b}$$

which lead to the Landau-Lifshitz-Gilbert (LLG) equations

$$\begin{aligned}\hbar S\sin\theta\partial_t\theta=&-JS^2a_0^2\left\{\sin^2\theta\partial_z^2\varphi+\sin 2\theta\,(\partial_z\varphi)(\partial_z\theta)\right\}\\&+DS^2a_0\sin 2\theta\,(\partial_z\theta)-\tilde{H}_xS\sin\theta\sin\varphi\\&+\alpha\hbar S\sin^2\theta(\partial_t\varphi),\end{aligned} \tag{9a}$$

$$\begin{aligned}\hbar S\sin\theta\partial_t\varphi=&\,JS^2a_0^2\left\{\partial_z^2\theta-\tfrac{1}{2}\sin 2\theta\,(\partial_z\varphi)^2\right\}\\&+DS^2a_0\sin 2\theta\,(\partial_z\varphi)-\tilde{H}_xS\cos\theta\cos\varphi\\&+\tilde{H}_zS\sin\theta-\alpha\hbar S\partial_t\theta.\end{aligned} \tag{9b}$$

The LLG equations describe the individual (not collective) spin dynamics.

3. *Collective dynamics*

To consider the sliding motion of the CSL, we use the collective coordinate method[18] introduced in Ref. 8. In this formulation, the CSL dynamics is fully described by two dynamical variables, the center-of-mass position Z and the out-of-plane quasizero mode (OPQZ) coordinate ξ_0. Using them the sliding solution is written as

$$\varphi(z,t) = \varphi_0[z - Z(t)], \tag{10a}$$

$$\theta(z,t) = \pi/2 + \xi_0(t) u_0[z - Z(t)]. \tag{10b}$$

The zero-mode wave function

$$u_0(z) = \sqrt{\frac{K}{LE}}\,\mathrm{dn}\left(\frac{\pi Q_0}{4E} z\right) = \frac{2}{\pi Q_0}\sqrt{\frac{KE}{L}}\,\partial_z\varphi_0(z) \tag{11}$$

serves as the basis function of the θ fluctuations localized around each soliton and $\xi_0(t)$ is the OPQZ *coordinate*. Here dn is the Jacobi dn function. The function $u_0(z)$ exactly corresponds to the topological charge distribution because a phase gradient $\partial_z\varphi_0(z)$ represents a topological charge localized around each soliton. Using these variables, the Lagrangian $\mathcal{L} = \int dz\tilde{\mathcal{L}}$ and the Rayleigh term $\mathcal{W} = \int dz\tilde{\mathcal{W}}$ are respectively written as

$$\mathcal{L} = \frac{\hbar S}{a_0^3}\mathcal{K}\xi_0\dot{Z} - \frac{\varepsilon_0^{(\theta)}}{a_0^3}\xi_0^2 + \frac{S\sqrt{L}}{a_0^3}\tilde{H}_z\xi_0 \tag{12}$$

and

$$\mathcal{W} = \frac{\alpha\hbar S}{2a_0^3}\left(\mathcal{M}\dot{Z}^2 + \dot{\xi}_0^2\right), \tag{13}$$

where $\mathcal{K} = \int_0^L dz u_0(z)\partial_z\varphi_0(z)$ and $\mathcal{K} = \int_0^L dz[\partial_z\varphi_0(z)]^2$ as given in Ref. 8. Furthermore, $\varepsilon_0^{(\theta)} \simeq D^2S^2/2J$ is an energy gap of the θ mode caused by the DM interaction which plays the role of an easy-plane anisotropy. We here note the useful relation

$$\varepsilon_0^{(\theta)}/\tilde{H}_c = 8S/\pi^2 \tag{14}$$

[see Eq. (16) of Ref. 8]

Under the weak-field condition, $\kappa \ll 1$, we have $\mathcal{K} \simeq Q_0\sqrt{L}$ and $\mathcal{M} \simeq Q_0^2 L$. We have $\xi_0(t) \neq 0$ only for nonequilbrium states where the CSL exhibits sliding motion. The emergence of such coherent collective transport in nonequilibrium states is a manifestation of the dynamical off-diagonal long-range order. Using Eqs. (10a) and (10b), Eqs. (9a) and (9b) lead to the equations of motion (EOMs) for the collective dynamics,

$$\hbar\mathcal{K}\dot{\xi}_0 = -\alpha\hbar\mathcal{M}\dot{Z}, \tag{15a}$$

$$\hbar\mathcal{K}\dot{Z} = 2S^{-1}\varepsilon_0^{(\theta)}\xi_0 + \alpha\hbar\dot{\xi}_0 - \sqrt{L}\tilde{H}_z. \tag{15b}$$

This set of EOMs differs from Eqs. (37) given in Ref. 8 in that the *sd* interaction is absent and a longitudinal field is present. In Ref. 8, the incoherent driving of the CSL sliding motion was caused by spin torque transfer from the spin-polarized current to the local spins. On the other hand, in the present case, we are discussing coherent driving caused by a uniform time-dependent magnetic field $\tilde{H}_z$.

Equations (15a) and (15b) are readily solved to give

$$\dot{Z}(t) = Ce^{-t/\tau_{\mathrm{CSL}}} - \frac{e^{-t/\tau_{\mathrm{CSL}}}}{(1+\alpha^2)\hbar Q_0}\int^t e^{t'/\tau_{\mathrm{CSL}}}\frac{d\tilde{H}_z(t')}{dt'}dt', \tag{16a}$$

$$\xi_0(t) = De^{-t/\tau_{\mathrm{CSL}}} + \frac{\alpha\sqrt{L}e^{-t/\tau_{\mathrm{CSL}}}}{(1+\alpha^2)\hbar}\int^t e^{t'/\tau_{\mathrm{CSL}}}\tilde{H}_z(t')dt', \tag{16b}$$

where we used the relation $\mathcal{M}/\mathcal{K}^2 = 1$ for a weak field. The constants C and D are determined by the initial conditions $\dot{Z}(0) = 0$ and $\xi_0(0) = 0$. The intrinsic relaxation time of the CSL, caused by the Gilbert damping, is introduced by

$$\tau_{\mathrm{CSL}} = \frac{\hbar S(\alpha+\alpha^{-1})}{2\varepsilon_0^{(\theta)}} \simeq \frac{\hbar(\alpha+\alpha^{-1})}{S}\frac{J}{D^2}, \tag{17}$$

which is also written as

$$1/\tau_{\mathrm{CSL}} \simeq \alpha\omega_{\mathrm{gap}}, \tag{18}$$

with $\omega_{\mathrm{gap}} = \varepsilon_0^{(\theta)}/\hbar$ being the characteristic frequency of the gap. In the case of static $\tilde{H}_z$, we have trivial relaxational dynamics where the sliding motion never persists. Furthermore, the DM interaction D gives rise to a finite relaxation time. Equation (16b) means that the longitudinal field first directly couples to ξ_0 and drives its growth via the Gilbert damping process. Then, the sliding motion follows the growth of ξ_0. This process is consistent with intuitive ideas developed by Döring.[10]

We here emphasize that the two coordinates ξ_0 and Z are coupled to each other via the Gilbert damping α [see Eq. (15a)]. If there were no damping, we would have no correlated dynamics. This fact means that the CSL never realizes dissipationless collective motion. As we will see in Sec. V and Appendix C, the presence of the damping is essential to drive the SMF.

4. *Comparison of material parameters to theoretical formulas*

It may be worthwhile to summarize the relation between experimental data and theoretical parameters by taking the example of $Cr_{1/3}NbS_2$,[5] and theoretical formulas. In this sample, it is reported that $a_0 = 1.212 \times 10^{-9}$ m and $L_{\mathrm{CHM}} = 2\pi/Q_0 = 4.8 \times 10^{-8}$ m. The Cr atoms are in the trivalent state and have localized electrons with spins of $S = 3/2$. The observed critical field is $H_c = 2300$ Oe corresponding to 0.31 K. We have an estimation for the ratio $D/J = \tan(Q_0 a_0) = 0.16$. Another important quantity is the excitation gap, which is estimated as $\varepsilon_0^{(\theta)} \simeq 0.38$ K by using Eq. (14). The intrinsic relaxation time of the CSL is also estimated as $\tau_{\mathrm{CSL}} \simeq (\alpha+\alpha^{-1}) \times 3.0 \times 10^{-11}$ s. A small damping such as $\alpha \simeq 10^{-2}$ leads to $\tau_{\mathrm{CSL}} \sim 3.0 \times 10^{-9}$ s. Smaller damping causes a longer relaxation time. To realize a longer period of the relaxation processes, it is desirable to have a smaller value of α and a smaller gap frequency ω_{gap}.

B. Static deformation of the CSL

Now that we have set up all the necessary equations for the dynamics, we proceed with the stability analysis of the CSL

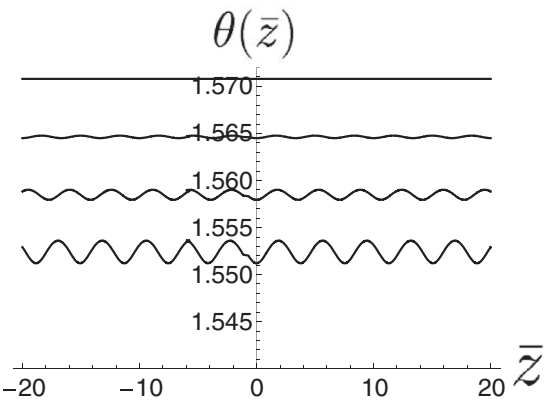

FIG. 2. Spatial modulation of $\theta(\bar{z}) = \pi/2 + \theta_1(\bar{z})$ for $\tilde{H}_x/\tilde{H}_c = 0,0.1,0.2,0.3$ (from top to bottom), keeping $\tilde{H}_z/\tilde{H}_x = 0.1$. Here the dimensionless coordinate $\bar{z} = \pi Q_0 z/4E$ is used.

against crossed magnetic fields. Before going to dynamical deformation, it is worthwhile to study the static deformation. For the analysis, we here consider the weak-field limit $|\tilde{H}_x| \ll JS$ and $|\tilde{H}_z/\tilde{H}_x| \ll 1$.

We introduce the static deformations as $\theta(z) = \pi/2 + s\tilde{\theta}(z)$ and $\varphi(z) = \varphi_0(z) + s\tilde{\varphi}(z)$, with the small fluctuations $\tilde{\theta}$,$\tilde{\varphi}$ and s being a dummy expansion parameter. As derived in Appendix A, we have

$$\tilde{\theta}(\bar{z}) = \frac{\tilde{H}_z}{\tilde{H}_x}\frac{\kappa^2}{W}[C_1\tilde{\varphi}_1(\bar{z}) + C_2\tilde{\varphi}_2(\bar{z})], \tag{19}$$

where the Wronskian W is given in Eq. (A7) and the coefficients $C_{1,2}$ are given by Eqs. (A11) and (A12). The functions $\tilde{\varphi}_{1,2}$ are a pair of fundamental solutions of the Lamé equation [Eq. (A2)]. In Fig. 2 we show the obtained spatial modulation of $\theta(\bar{z}) = \pi/2 + \theta_1(\bar{z})$ for various $\tilde{H}_z/\tilde{H}_c$, keeping $\tilde{H}_x/\tilde{H}_z = 0.1$. Since the coefficients $c_{1,2n}$ fall exponentially with growth of n, we retain only the terms with $n = \pm 1$, which dominate the terms with $|n| \geqslant 2$. We see that finite $\tilde{H}_z$ tends to orient the spins toward the z direction but causes *nonuniform* spatial oscillation. This oscillation implies that the static deformation considered here is unstable against dynamic deformation. We will see that this dynamic deformation corresponds to the sliding motion of the CSL.

III. COHERENT SLIDING DYNAMICS IN CROSSED MAGNETIC FIELDS

A. Energy and momeutum associated with the sliding motion

In this section we will show that the static deformation of the CSL is unstable against the dynamical instability, i.e., spontaneous coherent sliding motion of the whole CSL. As the present authors previously pointed out,[19] the Lagrangian constructed from the Hamiltonian Eq. (3) has hidden Galilean symmetry induced through Lie analysis.

This hidden symmetry justifies the assumption that the CSL has a linear momentum

$$P_z = \frac{\hbar S}{a_0^3}\int dz\,(1-\cos\theta)\,\partial_z\varphi \tag{20}$$

associated with the kinematic Berry phase. We connect the momentum variation δP_z to the energy variation,[20]

$$\delta E = \int dz\left(\frac{\partial\mathcal{H}}{\partial\theta}\delta\theta + \frac{\partial\mathcal{H}}{\partial\varphi}\delta\varphi\right) \tag{21}$$

associated with the sliding motion. In the absence of dissipation, plugging the EOMs (8a) and (8b) into Eq. (21), we have

$$\delta E = \hbar S\int dz\sin\theta\left(\frac{\partial\theta}{\partial t}\delta\varphi - \frac{\partial\varphi}{\partial t}\delta\theta\right). \tag{22}$$

The sliding motion means that θ and $\varphi$are functions of $u = z - Z(t)$ and we can make the replacement $\partial_t \to -\dot{Z}\partial_u$, $\partial_z \to \partial_u$. Then we easily obtain the relation

$$\delta E = \dot{Z}\delta P_z. \tag{23}$$

Based on this relation, we see that coherent sliding occurs if the condition $\dot{Z}\delta P_z < 0$ is satisfied for a given momentum transfer δP_z from the environment. We will see that in the present case the longitudinal magnetic field H_z causes the momentum transfer and drives the sliding motion.

B. Coherent sliding caused by a transient longitudinal field

We first consider a transient longitudinal field

$$H_z(t) = H_{z0}(1 - e^{-t/T}) \tag{24}$$

switched on in addition to the perpendicular static field H_x which stabilizes the CSL. Equation (16a) gives the sliding velocity

$$\dot{Z}(t) = -V_0\frac{\tau_{\rm CSL}}{\tau_{\rm CSL} - T}(e^{-t/\tau_{\rm CSL}} - e^{-t/T}), \tag{25}$$

where the characteristic velocity is defined by

$$V_0 = \frac{\tilde{H}_{z0}}{\hbar Q_0(1+\alpha^2)}. \tag{26}$$

Equation (25) indicates that $\dot{Z} < 0$ for $T < \tau_{\rm CSL}$ and then the condition $\dot{Z}\delta P_z < 0$ is satisfied. It is to be noted that if the chirality of the crystal were inverted, i.e., Q_0 were inverted to $-Q_0$, the velocity would be inverted. So *the sliding orientation and the crystal chirality correlate with each other.*

In the case of $Cr_{1/3}NbS_2$, the characteristic velocity is estimated as $V_0 \simeq 0.13\ \mathrm{m\,s^{-1}\,Oe^{-1}}$]. So, the sudden switching of the longitudinal magnetic field H_z, satisfing the condition $T < \tau_{\rm CSL}$, will easily cause the coherent sliding motion the CSL.

In Fig. 3, we show the time evolution of the sliding velocity. We see that the velocity grows linearly with time shortly after the field H_z is switched on. Then, after the relaxation time of the field, T, the velocity begins to relax. It finally relaxes to zero over the time scale of the Gilbert damping, $\tau_{\rm CSL}$. Therefore, to realize a longer-lasting sliding motion, a smaller value of α and a smaller gap frequency $\omega_{\rm gap}$ may be desirable.

C. Coherent oscillating motion under an ac field

It is also possible that an oscillating longitudinal field

$$H_z(t) = H_{z1}\sin(\Omega t) \tag{27}$$

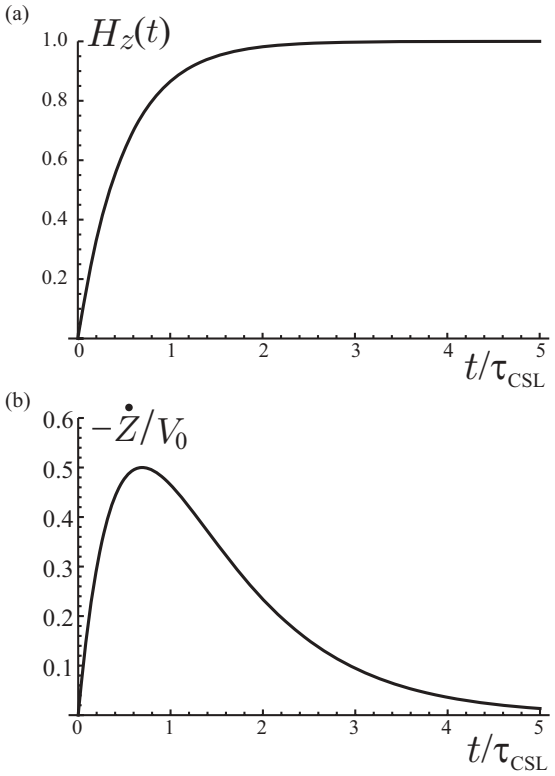

FIG. 3. Time dependence of (a) longitudinal field $H_z(t) = H_{z0}(1 - e^{-t/T})$ and (b) velocity $\dot{Z}/V_0$ for $T = 0.5\tau_{CSL}$.

causes a coherent oscillating motion of the CSL in addition to a perpendicular static field H_x. In this case, Eq. (16a) gives the velocity

$$\dot{Z}(t) = V_1[e^{-t/\tau_{CSL}} - \Omega\tau_{CSL}\sin(\Omega t) - \cos(\Omega t)], \quad (28)$$

where the characteristic velocity is defined by

$$V_1 = \frac{\tilde{H}_{z1}\Omega\tau_{CSL}}{\hbar Q_0(1+\alpha^2)\left(1+\tau_{CSL}^2\Omega^2\right)}. \quad (29)$$

Unlike the case of the transient field, here the oscillational sliding motion is sustained as a long-term stationary state. This is because in the ac case the energy associated with the CSL motion is perpetually supplied by the ac field. It is also seen that the Gilbert damping causes out-of-phase oscillations [$\cos(\Omega t)$]. For experiment, it may be useful to note that

$$\frac{V_1}{V_0} = \frac{\Omega\tau_{CSL}}{\left(1+\tau_{CSL}^2\Omega^2\right)}\frac{\tilde{H}_{z1}}{\tilde{H}_{z0}}. \quad (30)$$

In Fig. 4, we show the oscillating response of the sliding velocity to the longitudinal ac field. The transient state rapidly relaxes over the time scale of T to the stationary forced oscillation with a phase shift due to the damping.

Here we comment on the relation of the sliding dynamics to the electron spin resonance (ESR).[7] Provided the whole CSL is in a state of rest, the longitudinal ac field is able to excite a small-amplitude phononlike mode (a chiral soliton lattice phonon or magnetic kink crystal phonon) propagating over the CSL. However, because the ac field is uniform, resonant phonon absorption occurs only when the momentum absorbed by the phonon coincides with the reciprocal vector of the

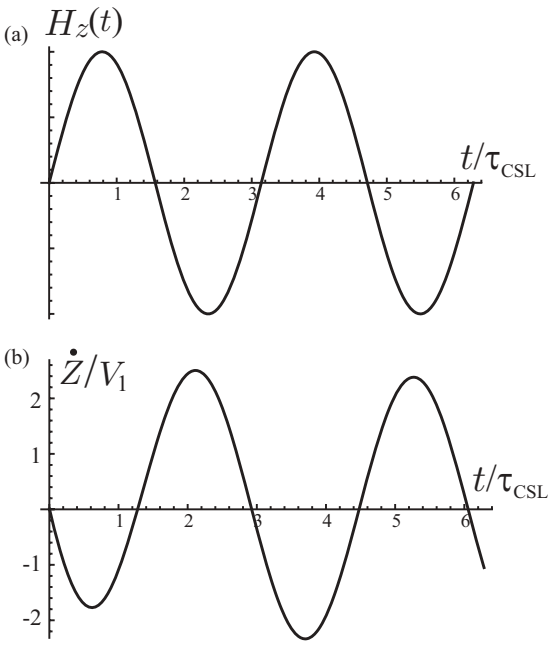

FIG. 4. Time dependence of (a) longitudinal field $H_z(t) = H_{z1}\sin(\Omega t)$ and (b) velocity $\dot{Z}/V_0$ for $\Omega^{-1} = 0.5\tau_{CSL}$.

super-Brillouin zone of the CSL. Once the resonance condition is satisfied, the microwave energy is consumed to excite the CSL phonons. On the other hand, in the case of off-resonant absorption, the sliding motion is driven. We also note that the excitations associated with the fluctuations of φ are totally irrelevant to the CSL phonon excitation. On the other hand, the sliding motion is a consequence of the correlated dynamics of the coupled θ and φ.

IV. NUMERICAL ANALYSIS OF THE DYNAMICS

A. Static deformation of the CSL

So far we have discussed the CSL dynamics in an analytical manner. To justify the obtained results, it is desirable to perform numerical simulations of the dynamics. For numerical analysis, we start with the lattice version of Eqs. (9a) and (9b) written as

$$\frac{d\theta_i}{d\tau} = \sqrt{1+\frac{D^2}{J^2}}\sin\theta_{i-1}\sin(\varphi_i - \varphi_{i-1} + \delta) - \sqrt{1+\frac{D^2}{J^2}}\sin\theta_{i+1}\sin(\varphi_{i+1} - \varphi_i + \delta) - \beta_x\sin\varphi_i, \quad (31a)$$

$$\frac{d\varphi_i}{d\tau} = -(\cos\theta_{i+1} + \cos\theta_{i-1}) + \sqrt{1+\frac{D^2}{J^2}}\cot\theta_i\sin\theta_{i-1}\cos(\varphi_i - \varphi_{i-1} + \delta) + \sqrt{1+\frac{D^2}{J^2}}\cot\theta_i\sin\theta_{i+1}\cos(\varphi_{i+1} - \varphi_i + \delta) - \beta_x\cot\theta_i\cos\varphi_i + \beta_z, \quad (31b)$$

where $\delta = \arctan(D/J)$, $\beta_x = \tilde{H}_x/JS$, and $\beta_z = \tilde{H}_z/JS$. Here, the time scale $\tau_0 = \hbar/JS$, and the dimensionless time $\tau = t/\tau_0$ is introduced.

First we consider static spin configurations. In order to perform numerical computations, we adjust the problem to a form convenient for an iterative routine, i.e.,

$$\sin\varphi_i = (\mathcal{A}_{i+1} + \mathcal{B}_{i-1})[(\mathcal{A}_{i+1} + \mathcal{B}_{i-1})^2 + (\mathcal{C}_{i-1} + \mathcal{D}_{i+1} + \beta_x)^2]^{-1/2}, \quad (32)$$

$$\cos\varphi_i = (\mathcal{C}_{i-1} + \mathcal{D}_{i+1} + \beta_x)[(\mathcal{A}_{i+1} + \mathcal{B}_{i-1})^2 + (\mathcal{C}_{i-1} + \mathcal{D}_{i+1} + \beta_x)^2]^{-1/2}, \quad (33)$$

$$\cos\theta_i = (\cos\theta_{i+1} + \cos\theta_{i-1} + \beta_z)[(\cos\theta_{i+1} + \cos\theta_{i-1} + \beta_z)^2 + (\mathcal{A}_{i+1} + \mathcal{B}_{i-1})^2 + (\mathcal{C}_{i-1} + \mathcal{D}_{i+1} + \beta_x)^2]^{-1/2}, \quad (34)$$

where we defined

$$\begin{pmatrix} \mathcal{A}_i \\ \mathcal{B}_i \\ \mathcal{C}_i \\ \mathcal{D}_i \end{pmatrix} = \sqrt{1 + D^2/J^2}\sin\theta_i \begin{pmatrix} \sin(\varphi_i + \delta) \\ \sin(\varphi_i - \delta) \\ \cos(\varphi_i - \delta) \\ \cos(\varphi_i + \delta) \end{pmatrix}. \quad (35)$$

The spin configuration is found by using the original spin variables and iteratively pointing each along the effective local field due to its neighbors. Scanning linearly through the chain, the spin variable at each site is updated in sequence, being reset along the net field due partly to some unchanged neighbors and to some that have already been reoriented. This gives convergence more quickly than a synchronized global update.

The most difficult computational problem in carrying out this program is to find the initial configuration that relaxes to a target spin configuration. It is meaningful to impose appropriate boundary conditions too. Obviously this is a rich problem with a wide choice of options. In our simulations we choose the starting configuration as the simple spiral $\varphi_i = q(i - z_0)$ and $\theta_i = \pi/2$, and take free boundary conditions. The coordinate z_0 corresponds to a position with $\varphi_i = \pi$ in the middle of a chain of length L. The value of $q = 0.1$ is taken throughout the numerical calculations to make more apparent the spatial modulation of solutions.

The convergence of the iteration process is very slow. The iterations stop if the sum

$$\sigma = \sqrt{\sum_{i=1}^{L}\left(\varphi_i^{(k)} - \varphi_i^{(k-1)}\right)^2 + \sum_{i=1}^{L}\left(\theta_i^{(k)} - \theta_i^{(k-1)}\right)^2} \quad (36)$$

taken over the chain on the kth step is less than the tolerance 10^{-8}. To reach this accuracy, around 205×10^6 iterations are required.

The numerical behavior of θ shown in Fig. 5 reproduces the theoretical findings (see Fig. 2), i.e., an increase of the longitudinal field enhances the modulation of the conical structure along the z axis. The calculation confirms another assumption of Sec. II A3, namely, the longitudinal field causes no changes in the variable φ (Fig. 6). The numerical data are imposed on the theoretical predictions [Eq. (19)] as shown in Fig. 7. Evidently, they reveal a good agreement with each other (Fig. 7).

B. Dynamics

A search for dynamical solutions is carried out by using the eighth-order Dormand-Prince method implemented in Ref. 21.

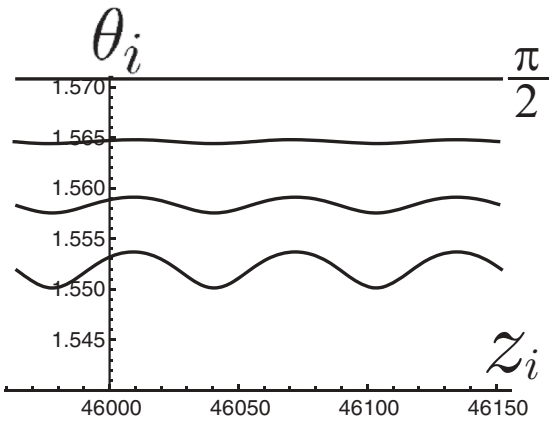

FIG. 5. Numerical dependence of θ on the coordinate z. The length of the chain is $L = 10^5$ sites. The calculation is performed with the same parameters as in Fig. 2. The perpendicular field $H_x/H_c = 0, 0.1, 0.2, 0.3$ (from top to bottom) is normalized to the critical field H_c.

The embedded Runge-Kutta integrator with an adaptive step-size control ensures a relative tolerance 10^{-12}. The integration spans a period of time from zero to $2 \times 10^4\,\tau_0$. The length of chains used in the computations amounts to $10^5 + 1$ sites. The time evolution of the magnetization was monitored by recording the time dependencies of the θ and φ variables for the central site.

In Fig. 8, we show the numerical results for the velocity. It is seen that the velocity decreases linearly with increasing β_z field. In the calculations β_x was held constant.

Figures 9 and 10 show the time dependences of θ and φ, respectively, under oscillating β_z for different values of the damping parameter α. These calculations make evident a salient feature of the forced oscillations. In the initial stage of time evolution, the longitudinal magnetic field excites intrinsic eigenmodes that are superimposed on the field-driven oscillations. The eigenmodes fade away in the steady-state regime and they are damped more rapidly the greater is the parameter α. The period of the forced oscillations $2\pi/\Omega$ exactly corresponds to the period of the driving force. In

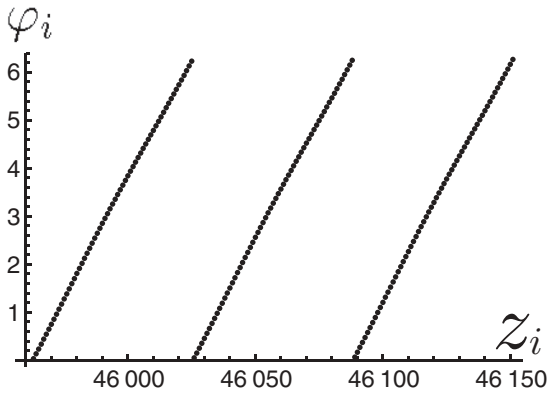

FIG. 6. Coordinate dependence of φ (shown as mod2π) obtained numerically for the chain of length $L = 10^5$ sites at the same parameters as in Fig. 2, and $H_x/H_c = 0.1$. From the almost strictly linear behavior, one sees that φ acquires almost no change.

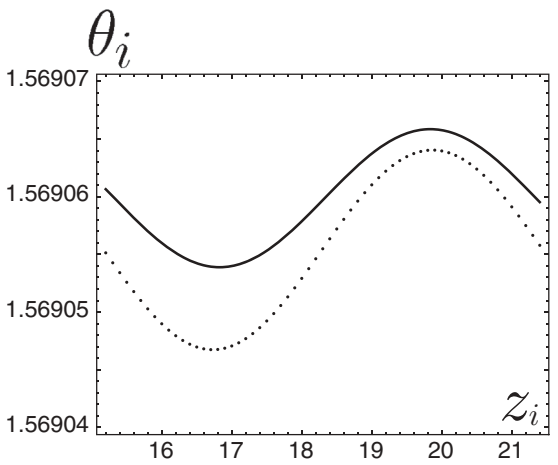

FIG. 7. A comparison between numerical data for the static case (dotted line) and the analytical expression given by Eq. (19) (solid line). The fields are $\beta_x = b\cos\delta_b$ and $\beta_z = b\sin\delta_b$, $b = 10^{-4}$, and $\delta_b = \pi/18$.

Appendix B, we present a detailed analysis of this forced oscillation in line with the numerical analysis.

V. SPIN MOTIVE FORCE

Now that we have obtained the CSL dynamics under crossed magnetic fields, we will go on to discuss possible SMF generation. Because the sliding motion of the CSL accompanies a dynamical deformation of the spin texture, we naturally expect the SMF to occur in the configuration presented in Fig. 1. Generally speaking, when the conduction electrons adiabatically experience a spatially modulated spin structure along the z axis, the spinor wave function locally follows the background. Consequently, the spinor space turns out to be curved. The corresponding curvature is represented by the gauge (Berry) connections. In the adiabatic picture, the Berry curvature in the spinor space acts as an effective electric field,[22,23]

$$E_\sigma(z,t) = -\frac{\hbar\sigma}{2e}\Omega_{zt} = \frac{\hbar\sigma}{2e}\sin\theta\,(\partial_z\theta\,\partial_t\varphi - \partial_z\varphi\,\partial_t\theta)\,. \tag{37}$$

Then we obtain a general expression for the SMF given by

$$\varepsilon_\sigma(t) = \int_0^L dz\,E_\sigma(z,t) = \frac{\hbar\sigma}{2e}\frac{d}{dt}\left(\int_\Gamma \cos\theta\, d\varphi\right), \tag{38}$$

where the contour Γ is taken on the sphere presenting a space of the order parameter $\boldsymbol{n}$. The voltage is related via the Stokes theorem to a change of area (Berry cap) $\mathcal{S}$ on the sphere enclosed by the contour,[24]

$$\varepsilon_\sigma(t) = -\frac{\hbar\sigma}{2e}\frac{d\mathcal{S}}{dt}. \tag{39}$$

This involves an analog of Faraday's law for the emergent electromagnetic field, where the magnetic field of a Dirac monopole with a charge $\hbar/2$ plays the role of the flux enclosed by the Berry cap $\mathcal{S}$.

In the present case of CSL dynamics, by using the collective representation [Eqs. (10a) and (10b)], the SMF for majority spins (the case of minority spins has the opposite sign) is computed as

$$\varepsilon(t) \simeq -\frac{\hbar}{2e}Q_0\dot{\xi}_0(t)\int_0^L u_0(z)dz. \tag{40}$$

This expression indicates that *the SMF arises only for* $\dot{\xi}_0 \neq 0$, i.e., the time dependence of the Berry cap is essential in causing the SMF (see Fig. 11). This observation is consistent with the discussion given in Ref. 24.

Using Eq. (11), we obtain

$$\int_0^L u_0(z)dz = \frac{4}{Q_0}\sqrt{\frac{KE}{L}}\mathcal{Q}, \tag{41}$$

where

$$\mathcal{Q} = \frac{\varphi_0(L) - \varphi_0(0)}{2\pi}, \tag{42}$$

is the topological charge representing the number of solitons over the whole length of a sample. Using the relation, $\dot{\xi}_0 = -\alpha Q_0\sqrt{L}\dot{Z}$, obtained from Eqs. (15a) and (40) finally reduces to

$$\varepsilon(t) \simeq \mathcal{Q}\frac{\hbar}{e}\pi\alpha Q_0\dot{Z}(t), \tag{43}$$

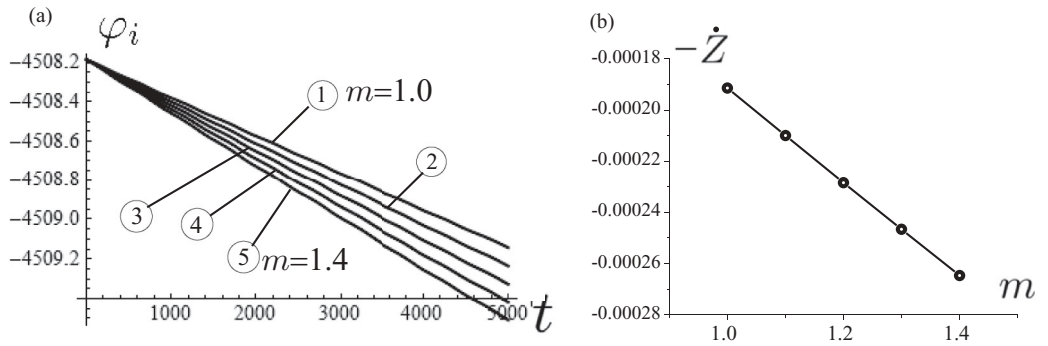

FIG. 8. (a) Linear time dependence of $\varphi(t)$ for the central site of a chain of length $L = 1\,000\,001$ obtained by numerical simulations. The fields are $\beta_x = b\cos\delta_b$ and $\beta_z = mb\sin\delta_b$, $b = 10^{-3}$, and $\delta_b = \pi/18$. With growth of β_z (or m) the slopes of the curves increase linearly according to the analytical result. The lines correspond to $m = 1.0$–1.4 with the step size 0.1, from top to bottom. (b) The dependence of $\dot{Z}$ on the factor m extracted from the $\varphi(t)$ data.

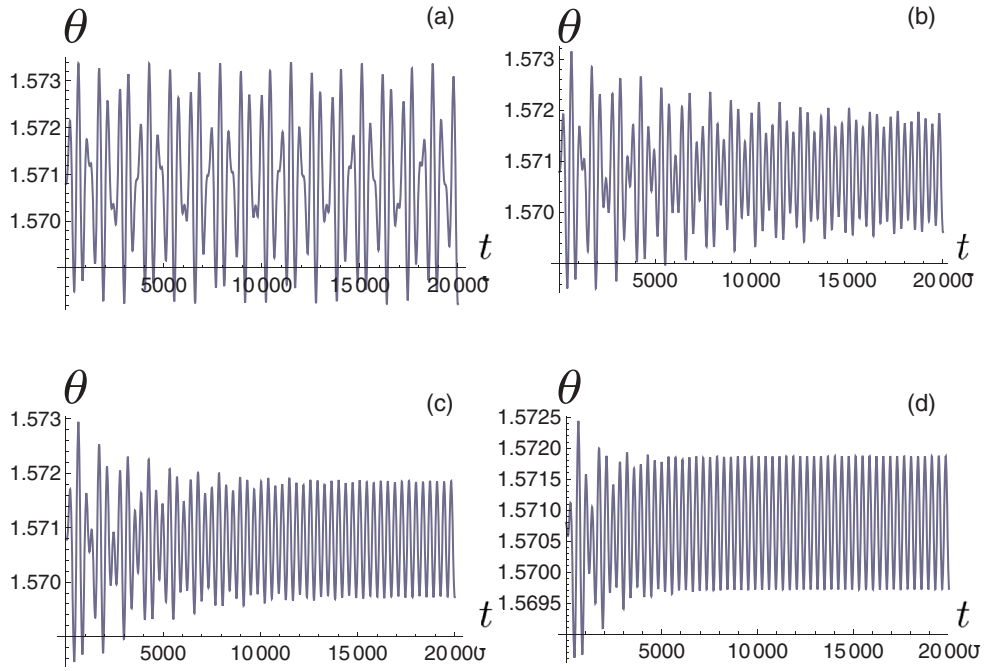

FIG. 9. (Color online) The time-dependent variation of θ for different damping parameters: (a) $\alpha = 0$, (b) $\alpha = 0.01$, (c) $\alpha = 0.02$, and (d) $\alpha = 0.05$. The fields are $\beta_x = b\cos\delta_b$ and $\beta_z = -b\sin\delta_b$, $b = 10^{-3}$, $\delta_b = \pi/18$, and the ratio β_z/Ω equals 0.01.

where we used the relation $\sqrt{KE} \simeq \pi/2$ in the case of a weak transverse field. As expected, the SMF is directly proportional to the macroscopic number of solitons, $\mathcal{Q}$. It is worthwhile to compare the obtained formula [Eq. (43)] with the one used for the SMF induced by domain wall motion.[24] In the present case of the CSL, the SMF is strongly amplified by the prefactor $\mathcal{Q}$. Furthermore, it should be stressed that *the dissipative dynamics is essential to drive the SMF.* Actually, the SMF is proportional to the Gilbert damping parameter α. In Appendix C, we show that the dissipationless rigid motion of the CSL never produces a SMF.

In the case of the time-dependent longitudinal field $H_z(t) = H_{z0}(1 - e^{-t/T})$, plugging Eq. (25) into Eq. (43), we immediately obtain

$$\varepsilon(t) \simeq -\varepsilon_0 \frac{\tau_{\mathrm{CSL}}}{\tau_{\mathrm{CSL}} - T}(e^{-t/\tau_{\mathrm{CSL}}} - e^{-t/T}), \tag{44}$$

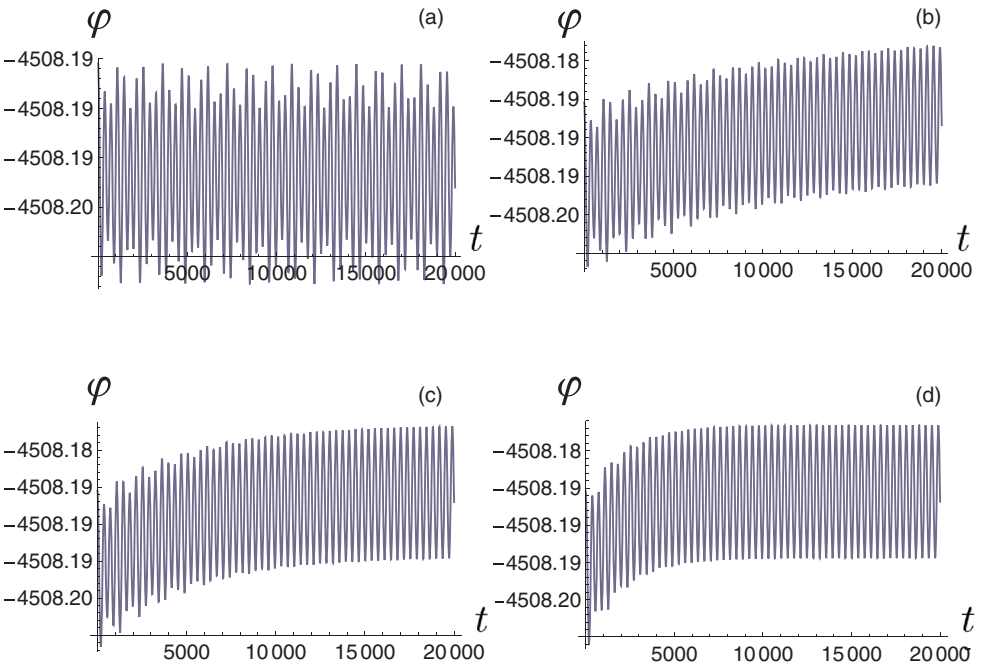

FIG. 10. (Color online) The time-dependent variation of the intrinsic mode of φ for different damping parameters: (a) $\alpha = 0$, (b) $\alpha = 0.01$, (c) $\alpha = 0.02$, and (d) $\alpha = 0.05$. The fields and frequency are the same as in Fig. 9.

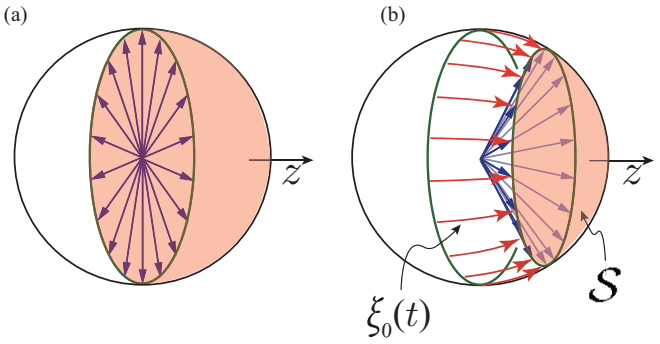

FIG. 11. (Color online) Switching of the time-dependent longitudinal field $H_z(t)$ causes a change in the Berry cap $\mathcal{S}$ from (a) to (b) in a time-dependent manner. This time dependence causes the SMF along the chiral axis. Each arrow represents a local spin configuration $\boldsymbol{n}(z)$. The Berry cap is associated with the area traced out by $\boldsymbol{n}(z)$.

where

$$\varepsilon_0 = \alpha \mathcal{Q} \frac{\hbar}{e} \pi Q_0 V_0. \tag{45}$$

In $Cr_{1/3}NbS_2$, using $Q_0 \simeq 1.3 \times 10^8$ m^{-1} and $V_0 \simeq 0.13$ m^{-1} s^{-1} Oe^{-1} as estimated in Sec. III B and assuming $\alpha \simeq 10^{-2}$, we have the estimation $\varepsilon_0 \simeq 0.36 \mathcal{Q} H_{z0}$ nV when H_{z0} is measured in oersteds. In the case where the sample size is $L \simeq 1$ mm, the upper bound of $\mathcal{Q}$ along the helical axis amounts to $L/L_{\rm CHM} \simeq 10^5$. Therefore, we expect that ε_0 amounts to 1 mV for $H_{z0} \simeq 10^2$ Oe as an example. To experimentally sustain the SMF, it may be desirable to apply a sequence of pulsed fields.

Here we comment on the physical reason why the SMF is proportional to the Gilbert damping factor α in Eq. (45). An essential point is that emergence of the SMF is a direct consequence of the time-varying Berry cap,[24] which needs a finite ξ_0. Now, as is clearly seen from the basic EOMs (15a) and (15b) if the Gilbert damping were absent, ξ_0 and Z would be dynamically decoupled and consequently $\xi_0 = \xi_0(0) = 0$ for all times, i.e., the sliding motion could never be sustained. This situation is totally different from the case of a 180° Bloch wall. The CSL is regarded as an array of 360° walls and we need some mechanism which enables the magnetic moments to rotate around the chiral axis. The only possible mechanism to realize this rotation is the Gilbert damping process. This is the reason why the SMF is proportional to α. More intuitively speaking, at the first stage the longitudinal field H_z directly couples to ξ_0 and causes the out-of-plane canting of the magnetic moments [see the Lagrangian (12)]. At the second stage, because of the Gilbert damping, the magnetic moments start a damped precession to relax back into their original directions. This motion triggers the rotation of the moments around the chiral axis and eventually leads to collective sliding.

VI. CONCLUDING REMARKS

In this paper, we demonstrated that the chiral soliton lattice exhibits coherent sliding motion by simple application of a *time-dependent* magnetic longitudinal field, in addition to a *static* transverse field. The driving force of the sliding is given by the Zeeman coupling of the collective coordinate ξ_0 with the longitudinal field. This mechanism is intuitively understood by Döring-Becker-Kittel (DBK) mechanism of the moving domain wall (DW).[10–12] In the DBK mechanism, once the domain wall begins to move, a so-called demagnetization field is dynamically generated inside the wall. The demagnetization field supplies spin torque to sustain the inertial motion. Actually, the DBK mechanism of a single DW has been analyzed by exactly the same procedure presented in this paper.[25] In the CSL dynamics, the longitudinal magnetic field kicks off the demagnetization and drives coherent sliding motion. To demonstrate the coherent sliding motion, we first used the collective coordinate method, and then confirmed the result by computational analysis.

The time duration of the sliding motion is characterized by the intrinsic relaxation time determined by Eq. (18). Providing the gap energy $\varepsilon_0^{(\theta)}$ varies between 0.1 and 10 K and the Gilbert damping constant varies between 10^{-4} and 10^{-2}, we expect the time duration to vary between 10^{-9} and 10^{-6} s. To realize longer-lasting sliding motion, a smaller value of α and a smaller gap frequency $\omega_{\rm gap}$ may be desirable. This estimation may give a guiding principle for materials synthesis. Sequential pluses of the longitudinal magnetic fields may remedy the quick decay of the sliding.

The sliding motion may be signaled by spin-density accumulation inside each soliton (kink) and the emergence of periodic arrays of induced magnetic dipoles carrying the transport spin current.[6] From the theoretical viewpoint, it is always possible for coherent sliding to occur as a direct consequence of the phase rigidity and Galilean symmetry in any type of density wave, including spin or charge density waves, and even inhomogeneous superconducting states. However, in many of such systems, the sliding motion does not transport an experimentally measured quantity.[26] In this respect, it is remarkable that the coherent sliding of the CSL accompanies dynamically generated magnetization.

Another observable consequence of the sliding is the appearance of the SMF along the helical axis. We showed that the time-dependent sliding velocity $\dot{Z}(t)$ causes a time-varying Berry cap which results in the SMF. We stressed that the dissipative dynamics plays an essential role in driving the SMF. A salient feature of the CSL is the appearance of a strongly amplified SMF which is directly proportional to the macroscopic number of solitons. Consequently, the SMF is expected to reach the order of millivolts. As reported in Ref. 5, the CHM state and the CSL are quite robust against structural dislocation and crystal defects. Their high stability and robustness are direct manifestations of the macroscopic order of the spin magnetic moments in the CHM and CSL states. We hope that the present proposal may lead to spintronics applications based on chiral magnetic crystals.

ACKNOWLEDGMENTS

J.K. acknowledges a Grant-in-Aid for Scientific Research (A) (No. 22245023) and a Grant-in-Aid for Scientific Research on Innovative Areas (No. 24108506) from the Ministry of Education, Culture, Sports, Science and Technology, Japan. Vl.E.S. acknowledges RFBR Grant No. 12-02-31565 mol_a. We acknowledge helpful discussions with Y. Togawa and J. Akimitsu.

APPENDIX A: STATIC DEFORMATION

Plugging the expressions, $\theta(z) = \pi/2 + s\tilde{\theta}(z)$ and $\varphi(z) = \varphi_0(z) + s\tilde{\varphi}(z)$ into the static counterparts of Eqs. (9a) and (9b), and retaining the first-order corrections with respect to s, we have

$$\partial_{\bar{z}}^2\tilde{\varphi} = (2\kappa^2 \mathrm{sn}^2\bar{z} - \kappa^2)\tilde{\varphi}, \tag{A1a}$$

$$\partial_{\bar{z}}^2\tilde{\theta} = (2\kappa^2 \mathrm{sn}^2\bar{z} - \kappa^2)\tilde{\theta} - \frac{\kappa^2}{\beta_x}\left(Q_0^2\theta_1 - \beta_z\right), \tag{A1b}$$

where the dimensionless variables $\bar{z} = \sqrt{\beta_x}z/\kappa$, $\beta_z = \tilde{H}_z/JS$, and $\beta_x = \tilde{H}_x/JS$ are introduced. Equation (A1a) is the homogeneous Lamé equation, while Eq. (A1b) is a nonhomogeneous Lamé equation. The solution of the Lamé equation is well known to be given in the form[27]

$$\tilde{\varphi}_{1,2}(\bar{z}) = \frac{H(\bar{z} \pm a)}{\Theta(\bar{z})}e^{\mp\bar{z}Z(a)}, \tag{A2}$$

where H and Z are Jacobi's eta and zeta functions, respectively, with the parameter a being determined by $\mathrm{dn}^2 a = -16E^2/\pi^2$.

A solution for the nonhomogeneous equation (A1b) is obtained by using the homogeneous solutions $\tilde{\varphi}_{1,2}$. In the inhomogeneous term, we ignore $Q_0^2\theta_1$ as compared with β_z. This treatment is justified because β_z and θ_1 are of the same order, and $Q_0 \ll 1$. Using the method of variation of parameters for a nonhomogeneous second-order differential equation, we readily construct the solution as

$$\tilde{\theta}(\bar{z}) = \frac{\beta_z}{\beta_x}\kappa^2 W^{-1}\left(\tilde{\varphi}_2(\bar{z})\int^{\bar{z}} d\bar{z}\,\tilde{\varphi}_1(\bar{z}) - \tilde{\varphi}_1(\bar{z})\int^{\bar{z}} d\bar{z}\,\tilde{\varphi}_2(\bar{z})\right), \tag{A3}$$

where W is the Wronskian,

$$W = \tilde{\varphi}_1(\bar{z})\tilde{\varphi}_2'(\bar{z}) - \tilde{\varphi}_2(\bar{z})\tilde{\varphi}_1'(\bar{z}). \tag{A4}$$

The Lamé equation guarantees that $dW/d\bar{z} = 0$, i.e., the Wronskian is independent of $\bar{z}$ and therefore $W = W(0)$. By plugging the expressions

$$\tilde{\varphi}_1(0) = -\tilde{\varphi}_2(0) = \frac{H(a)}{\Theta(0)} = \frac{\theta_1\left(\frac{\pi a}{2K}\right)}{\theta_4(0)} \tag{A5}$$

and

$$\tilde{\varphi}_1'(0) = \tilde{\varphi}_2'(0) = \frac{\pi}{2K}\frac{H'(a)}{\Theta(0)} - \frac{H(a)}{\Theta(0)}Z(a) \tag{A6}$$

into Eq. (A4), we finally obtain

$$W = \frac{2}{\vartheta_4^2}\theta_1^2\left(\frac{\pi a}{2K}\right)\left[\frac{\pi}{2K}\frac{\theta_1'\left(\frac{\pi a}{2K}\right)}{\theta_1\left(\frac{\pi a}{2K}\right)} - Z(a)\right], \tag{A7}$$

where $\theta_i(x)$ $(i = 1,2,3,4)$ denote the elliptic theta functions and $\vartheta_4 \equiv \theta_4(0) = \sqrt{2\kappa' K/\pi}$. Here κ' is the complementary modulus.

The final task is to perform the integrals in (A3) by using the Fourier transformation of $\tilde{\varphi}_{1,2}(\bar{z})$ to give Eq. (19). The derivation is similar to the calculation of Fourier coefficients for the Jacobi sn function.[27] We start with the Fourier transformation

$$\tilde{\varphi}_{1,2}(\bar{z}) = \sum_{n=-\infty}^{+\infty} c_{1,2n}e^{\bar{z}[i\pi n/2K \mp Z(a)]}. \tag{A8}$$

By definition, we have

$$2\pi c_{-n} = \int_{-\pi}^{\pi}\frac{\theta_1(x+a)}{\theta_4(x)}e^{\mathrm{inx}}\,dx.$$

To evaluate the integral, we use the contour taken as a parallelogram with the corner points $-\pi, \pi, \pi + \pi\tau$, and $-2\pi + \pi\tau$, where $\tau = iK'/K$. The singular points inside the contour are $z_1 = -\pi + \pi\tau/2$ and $z_2 = \pi\tau/2$. After straightforward computations, we obtain

$$c_{1,2n} = 0 \quad \text{for even } n, \tag{A9}$$

$$c_{1,2n} = -i\frac{\theta_4\left(\frac{\pi a}{2K}\right)}{\theta_1'\sinh[\pi(nK' \mp ia)/2K]} \quad \text{for odd } n. \tag{A10}$$

Finally we have

$$C_1 = -\sum_{n=-\infty}^{+\infty} c_{2n}\frac{e^{\bar{z}[i\pi n/2K + Z(a)]}}{\frac{i\pi n}{2K} + Z(a)}, \tag{A11}$$

$$C_2 = \sum_{n=-\infty}^{+\infty} c_{1n}\frac{e^{\bar{z}[i\pi n/2K - Z(a)]}}{\frac{i\pi n}{2K} - Z(a)}, \tag{A12}$$

where in the summation only terms with odd n are retained.

APPENDIX B: AC-FIELD-DRIVEN OSCILLATIONS OF THE CSL

We derive a solution of the LLG equations (9a) and (9b) for the periodic longitudinal magnetic field $\beta_z(\tau) = \beta_{z0}\sin\Omega\tau$. The solution is sought in the form $\theta = \pi/2 + \theta_1$ and $\varphi = \varphi_0 + \varphi_1$, where the additions θ_1 and φ_1 are of the same order of magnitude as the magnetic field β_z. To provide an analytical treatment, we consider the limit of small β_x when the approximations $\varphi_0(z) \approx Q_0 z$ and $\theta_0 = \pi/2$ are relevant. Moreover, we assume a small size of the Gilbert damping, when the problem becomes iterative. At the first stage, we find solutions for θ_1 and φ_1 at $\alpha = 0$ and plug them into Eqs. (9a) and (9b) to obatin new values valid for nonzero α.

At $\alpha = 0$ Eqs. (9a) and (9b) read as

$$\frac{\partial\theta_1}{\partial\tau} = -\frac{\partial^2\varphi_1}{\partial z^2} - \beta_x\cos Q_0 z\,\varphi_1, \tag{B1}$$

$$\frac{\partial\varphi_1}{\partial\tau} = -Q_0^2\theta_1 + \frac{\partial^2\theta_1}{\partial z^2} + \beta_x\cos Q_0 z\,\theta_1 + \beta_z \tag{B2}$$

and can be easily resolved through the substitutions

$$\begin{aligned}\varphi_1^{(0)}(z,\tau) &= (A_1 + A_2\beta_x\cos Q_0 z)\cos\Omega\tau,\\ \theta_1^{(0)}(z,\tau) &= (B_1 + B_2\beta_x\cos Q_0 z)\sin\Omega\tau,\end{aligned} \tag{B3}$$

where $A_{1,2}$ and $B_{1,2}$ are the unknowns.

This results straightforwardly in

$$\varphi_1^{(0)}(z,\tau) = -\left(\frac{\beta_{z0}}{\Omega} + \frac{\beta_{z0}}{\Omega}\frac{2\beta_x Q_0^2}{\left(2Q_0^4 - \Omega^2\right)}\cos Q_0 z\right)\cos\Omega\tau, \tag{B4}$$

$$\theta_1^{(0)}(z,\tau) = -\frac{\beta_x\beta_{z0}}{2Q_0^4 - \Omega^2}\cos Q_0 z\,\sin\Omega\tau. \tag{B5}$$

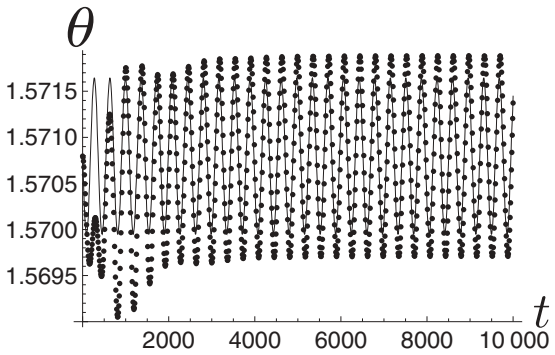

FIG. 12. The time-dependent variation of the polar angle for the central site ($N = 50\,000$): numerical data (dots) and analytical result (line) given by Eq. (B6). The fields are taken as in Fig. 8 in the main text; $\alpha = 0.1$.

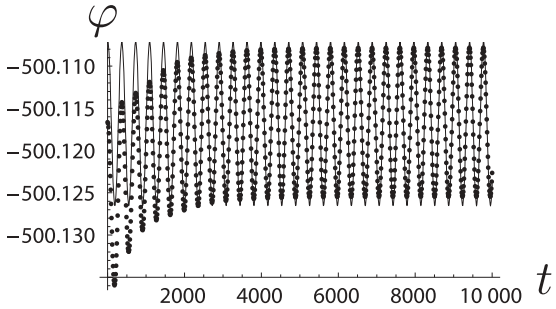

FIG. 13. The time-dependent variation of the azimuthal angle for the central site ($N = 50\,000$): numerical data (dots) and analytical result (line) given by Eq. (B7). The parameters are the same as in Fig. 12.

The requirement of smallness of the corrections amounts to $\beta_{z0} \ll \Omega$, $2\beta_x\beta_{z0}Q_0^2 \ll \Omega(2Q_0^4 - \Omega^2)$, and $\beta_x\beta_{z0} \ll 2Q_0^4 - \Omega^2$. Taking $Q_0 \sim 10^{-2}$ and $\Omega \sim 10^{-4}$ in dimensionless units (or 1 GHz in physical units for $\Omega\tau_0$), we can suppose, for example, $\beta_{z0}/\Omega \sim 0.1$, $\beta_x \sim 10^{-4}$ (100 Oe), and $\beta_{z0} \sim 10^{-5}$ (10 Oe).

By assuming smallness of the Gilbert parameter α, we organize the iterative procedure to find solutions of the system (9a), (9b) with the time derivatives in the right-hand sides estimated from Eqs. (B4) and (B5). The calculation yields

$$\theta_1(z,\tau) = \theta_1^{(0)}(z,\tau) - \alpha\frac{\beta_{z0}}{\Omega}\cos\Omega\tau \times\left[1 - \frac{\beta_x Q_0^2}{\Omega^2 - 2Q_0^4}\left(2 + \frac{3\Omega^2}{\Omega^2 - 2Q_0^4}\right)\cos Q_0 z\right], \tag{B6}$$

$$\varphi_1(z,\tau) = \varphi_1^{(0)}(z,\tau) + \alpha\frac{\beta_{z0}}{\Omega}\sin\Omega\tau\left[\frac{Q_0^2}{\Omega} - \frac{\beta_x\Omega}{\Omega^2 - 2Q_0^4} \times\left(1 + 2\frac{Q_0^4}{\Omega^2} + \frac{\Omega^2 + 4Q_0^4}{\Omega^2 - 2Q_0^4}\right)\cos Q_0 z\right]. \tag{B7}$$

A direct comparison between the numerical results and the analytical predictions is made in Figs. 12 and 13. Obviously, there is a good agreement in the steady-state regime, when the eigenmodes fade away.

APPENDIX C: ABSENCE OF SMF FOR RIGID MOTION

We here note that the dissipationless rigid motion of the CSL never causes SMF. The results can be obtained from general considerations. In Villain's representation,[28] the spin component $S^z = \hbar S\cos\theta$ and the angle φ made by the projection of the spin in the (x,y) plane are conjugated canonical variables. Equations (9a) and (9b) written in the new variables acquire the Hamiltonian form

$$\frac{\partial\varphi}{\partial t} = \frac{\partial\mathcal{H}}{\partial S^z}, \quad \frac{\partial S^z}{\partial t} = -\frac{\partial\mathcal{H}}{\partial\varphi}, \tag{C1}$$

whereas the fictitious electric field (37) is presented as

$$E(z,t) = \frac{1}{2S}\left(\frac{\partial S^z}{\partial t}\frac{\partial\varphi}{\partial z} - \frac{\partial S^z}{\partial z}\frac{\partial\varphi}{\partial t}\right). \tag{C2}$$

The spin motive force generated along the path of length L reduces to a contour integral in the phase space of the conjugated variables (φ, S^z),

$$\varepsilon(t) = \int_0^L dz\, E(z,t) = \frac{1}{2S}\oint_\Gamma\left(\frac{\partial S^z}{\partial t}d\varphi - \frac{\partial\varphi}{\partial t}dS^z\right) = -\frac{1}{2S}\int_S\left[\frac{\partial}{\partial\varphi}\left(\frac{\partial\varphi}{\partial t}\right) + \frac{\partial}{\partial S^z}\left(\frac{\partial S^z}{\partial t}\right)\right]d\varphi dS^z. \tag{C3}$$

Plugging Eqs. (C1) into this formula we obtain $\varepsilon(t) = 0$. This rigorous result shows that dissipationless Hamiltonian dynamics of any spin texture never causes finite SMF.

[1] E. B. Sonin, Adv. Phys. **59**, 181 (2010).
[2] I. Žutić, J. Fabian, and S. Das. Sarma, Rev. Mod. Phys. **76**, 323 (2004), and references therein.
[3] I. E. Dzyaloshinskii, Zh. Eksp. Teor. Fiz. **46**, 1420 (1964) [Sov. Phys. JETP **19**, 960 (1964)]; Zh. Eksp. Teor. Fiz. **47**, 992 (1964) [Sov. Phys. JETP **20**, 665 (1965)].
[4] J. Kishine, K. Inoue, and Y. Yoshida, Prog. Theor. Phys. Suppl. **159**, 82 (2005).
[5] Y. Togawa, T. Koyama, K. Takayanagi, S. Mori, Y. Kousaka, J. Akimitsu, S. Nishihara, K. Inoue, A. S. Ovchinnikov, and J. Kishine, Phys. Rev. Lett. **108**, 107202 (2012).
[6] I. G. Bostrem, J. I. Kishine, and A. S. Ovchinnikov, Phys. Rev. B **77**, 132405 (2008); **78**, 064425 (2008).
[7] J. I. Kishine and A. S. Ovchinnikov, Phys. Rev. B **79**, 220405(R) (2009).
[8] J. I. Kishine, A. S. Ovchinnikov, and I. V. Proskurin, Phys. Rev. B **82**, 064407 (2010).
[9] J. I. Kishine, I. V. Proskurin, and A. S. Ovchinnikov, Phys. Rev. Lett. **107**, 017205 (2011).
[10] W. Döring, Z. Naturforsch., A **3**, 374 (1948).
[11] R. Becker, in *Proceedings of the Grenoble Conference, 1950* (unpublished).
[12] C. Kittel, Phys. Rev. **80**, 918 (1950).
[13] S. E. Barnes and S. Maekawa, Phys. Rev. Lett. **98**, 246601 (2007).
[14] S. A. Yang, G. S. D. Beach, C. Knutson, D. Xiao, Q. Niu, M. Tsoi, and J. L. Erskine, Phys. Rev. Lett. **102**, 067201 (2009).

[15]P. N. Hai, S. Ohya, M. Tanaka, S. E. Barnes, and S. Maekawa, Nature (London) **458**, 489 (2009).
[16]J. Ohe, S. E. Barnes, H.-W. Lee, and S. Maekawa, Appl. Phys. Lett. **95**, 123110 (2009).
[17]Y. Yamane, K. Sasage, T. An, K. Harii, J. Ohe, J. Ieda, S. E. Barnes, E. Saitoh, and S. Maekawa, Phys. Rev. Lett. **107**, 236602 (2011).
[18]N. H. Christ and T. D. Lee, Phys. Rev. D **12**, 1606 (1975).
[19]I. G. Bostrem, J. Kishine, R. V. Lavrov, and A. S. Ovchinnikov, Phys. Lett. A **373**, 558 (2009).
[20]A. M. Kosevich, B. A. Ivanov, and A. S. Kovalev, Phys. Rep. **194**, 117 (1990).
[21]W. H. Press, S. A. Teukolsky, W. T. Vetterling, and B. P. Flannery, *Numerical Recipes*, 3rd ed. (Cambridge University Press, Cambridge, 2007).
[22]G. E. Volovik, J. Phys. C **20**, L83 (1987).
[23]Di Xiao, Ming-Che Chang, and Qian Niu, Rev. Mod. Phys. **82**, 1959 (2010).
[24]S. A. Yang, G. S. D. Beach, C. Knutson, D. Xiao, Z. Zhang, M. Tsoi, Q. Niu, A. H. MacDonald, and J. L. Erskine, Phys. Rev. B **82**, 054410 (2010).
[25]J. I. Kishine and A. S. Ovchinnikov, Phys. Rev. B **81**, 134405 (2010).
[26]This point is stressed by P. W. Anderson, *Basic Notions of Condensed Matter Physics* (Benjamin, Menlo Park, 1984), Sec. 4E.
[27]E. T. Whittaker and G. N. Watson, *A Course of Modern Analysis* (Cambridge University Press, New York, 1927).
[28]J. Villain, J. Phys. (Paris) **35**, 27 (1974).